Source Parameter Estimates for Small Earthquakes

Tetsu Masuda

Geophysical Institute, Faculty of Science,
Tôhoku University, Sendai 980, Japan

Akio Takagi

Observation Center for Earthquake Prediction, Faculty of Science,
Tôhoku University, Sendai 980, Japan

Abstract: The source parameters of seismic moment, fault radius, and stress drop of the small earthquakes near Miyako, Iwate Prefecture, northeastern part of Japan, with focal depths 32 km∼55 km are obtained from the spectra of P and SH waves. The spectra obtained here are amenable to the interpretation by the source model referred to in this study. We have observed that the P wave corner frequencies are systematically larger than the S wave corner frequencies, the ratios being 1.0∼1.7. Seismic moments, ranging from 10^{18} dyne-cm to 10^{21} dyne-cm, and the fault radii, from 0.05 km to 0.2 km, are well determined within the error of a factor of 2 and 20 percent, respectively, since the spectra are of simple shape. This is due to the near-vertical emergences of the seismic rays to the stations. The stress drops range from 1 bar to 40 bars. The data show some scatter, however, there is a tendency of increase in stress drop with increasing seismic moment. Our result suggests that the magnitude, or the seismic moment of the small earthquakes, scales with both the two factors of fault radius and stress drop.

1. Introduction

Owing to the advances in theoretical study of seismic source processes, our understanding of the dynamic mechanism of earthquakes has been much improved. The theoretical approach provides us with a practical basis in interpreting the observational results in terms of the physical properties in the source region. On the other hand, the recent development in the seismological observation system has brought us the informations of good quality, from which the shear dislocation models, rather simple they may be, have positively been justified. An advantageous aspect of shear dislocation models to our understanding of the earthquake source mechanism is that they can describe the source process with a few number of independent parameters. Recent works on seismic source modelling serve for clarification of quantitative relations between the spectral characteristics of the far-field seismic body waves and the average properties of the physical process at the source (Brune, 1970; Sato and Hirasawa, 1973; Masuda et al., 1977a). A prediction of these relations from a particular source model has been of practical use in estimating the source parameters of seismic moment, source dimension, released energy, and stress drop of earthquakes for which no evident field observations are available. Spectral analyses of seismic waves have successfully been applied for derivation of the gross properties of

seismic sources for large shocks (e.g., Hanks and Wyss, 1972; Trifunac, 1974; Izutani, 1974). Since the data for large shocks are available at many stations with a variety of azimuths and epicentral distances, the source paramenters, in particular seismic moment, can be fairly well determined. Scaling relations for seismic source parameters of large shocks have been discussed (Kanamori and Anderson, 1975; Geller, 1976), and it has been suggested that the earthquake magnitudes, or seismic moments, may scale with only one parameter of fault length. This implies that the sources of large shocks are geometrically similar and the stress drops take a constant value independent of earthquake magnitudes. Literatures have shown that the fault width of a half of fault length and the stress drop of several tens of bars are approximately adequate within the deviations of a factor of 4. The deviations may be due to some geological and tectonical localities and partly due to the uncertainty in estimating the source dimensions.

The existence of the above scaling relation suggests the dominance of the effect of general tectonic stress on the nature of the earthquake sources of large shocks. On the contrary, for small shocks, the characteristics of the source may be under influences of various factors of geological structure, material properties and others. It is an interesting problem to investigate the relations among source parameters, and to estimate the values of stress drop for small earthquakes. Recent results indicate a variety of values of stress drop for small earthquakes, raging from a few tenth to hundreds of bars, with a tendency of increase with increasing magnitude (Thatcher and Hanks, 1973; Johnson and McEvilly, 1974; Bakun et al., 1976).

This paper reports the source parameters estimated for small earthquakes near Miyako, Iwate Prefecture, northeastern part of Japan, and discusses on the source properties of these earthquakes. The earthquakes analysed here are located in a region of high seismic activity and on the upper sheet of the two deep seismic planes, the pattern of occurrence being temporally stable (Takagi and Hasegawa, 1976). Umino et al. (1976) and Hasegawa (1977) have shown that the upper sheet of the deep seismic planes corresponds to the structural boundary with high velocity contrast. The characteristics of the sources of these earthquakes involve many informations for understanding the physical mechanism of the tectonic system in the northeastern Japan.

2. Theoretical Basis

Shear dislocation models predict the gross characteristics of far-field displacement spectrum which is characterized by the constant low-frequency level Ω_0, and the high-frequency spectral asymptote $f^{-\gamma}$ beyond the corner frequency f_0. Hence the displacement spectrum is described by three basic parameters Ω_0, f_0, and γ. The physical parameters of the seismic source, seismic moment M_0 and fault radius R, may be estimated from the spectral parameters Ω_0 and f_0 according to the following relations;

$$M_0 = \frac{4\pi \rho r c^3 \Omega_0}{\mathscr{R}_{\theta\phi}} \, , \tag{1}$$

$$R = \frac{f'_{0c}\, c}{f_{0c}} \, , \tag{2}$$

where $\mathscr{R}_{\theta\phi}$ accounts for the radiation pattern of equivalent double couple source, r is the hypocentral distance, ρ and c are the density and the phase velocity of seismic waves at the source. Here the nondimensional quantity f_{0c}' depends upon the choice of a particular soruce model. Recently Masuda et al., (1977a) have given the values of f_{0c}' in modelling the seismic source for small earthquakes with a dynamic solutions of expanding shear cracks applied to circular faults. Their result shows an azimuthal dependence of f_{0c}', the average over azimuths being 0.16 and 0.17 for P and S waves, respectively. R may be then related to f_{0p} and f_{0s} as

$$R_p = \frac{0.16\alpha}{f_{0p}} \, , \tag{3}$$

$$R_s = \frac{0.17\beta}{f_{0s}} \, , \tag{4}$$

where α and β are the P and S wave velocity, respectively. As is evident in the equations, their model estimates the fault radius at a smaller value than those according to other source models. This is due to the dynamic features of source time function (Masuda et al., 1977b). The stress drop $\Delta\sigma$ of an earthquake is evaluated from M_0 and R as

$$\Delta\sigma = k\,\frac{M_0}{R^3} \, , \tag{5}$$

where $k=0.43$, the same value as derived by Keilis-Borok (1959). In this study, we refer to equations (1), (3), (4), and (5) in estimating the source parameters. The choice of their model is due to the idea that, for small earthquakes, the fault geometry of a circle may be appropriate for the first approximation to derive the gross properties of the seismic source, and that the model relates the fault radius to the corner frequency based upon the mathematical solutions of dynamic rupture problem.

3. Data Analysis and Seismic Source Spectra

Source parameters obtained in this study are estimated from the spectra of P and S waves of small earthquakes which occurred in the period from April to July of 1976. The epicentres of these earthquakes are confined in a narrow region near the Miyako station (**MYK**) in the Microearthquake Observation Network of Tôhoku University, the focal depths ranging from 32 km to 55 km. The magnitudes, determined from the total duration of signal, and the hypocentral parameters of the earthquakes are listed in Table 1, these values being routinely determined by the Observation Centre for Earthquake Prediction, Tôhoku University. The values in parenthesis indicate the

Table 1.

Date		h : m	m_{fp}	Lat (°N)	Long (°E)	Depth (km)
04	Apr.	19:48	2.1	39.753(0.008)	142.150(0.012)	33.5(1.7)
07	Apr.	15:26	1.0	39.755(0.020)	142.162(0.028)	33.1(4.2)
08	Apr.	19:54	1.5	39.681(0.048)	142.201(0.036)	34.7(4.7)
19	Apr.	08:00	1.9	39.682(0.015)	142.101(0.024)	44.1(2.3)
20	Apr.	05:29	1.1	39.706(0.013)	141.876(0.022)	47.0(1.9)
28	Apr.	16:27	3.0	39.648(0.010)	142.090(0.016)	45.1(1.4)
01	May.	17:09	1.3	39.684(0.018)	141.887(0.031)	47.0(2.6)
06	May.	23:22	2.4	39.700(0.011)	142.111(0.018)	44.2(1.8)
06	May.	23:25	2.2	39.702(0.011)	142.110(0.018)	44.0(1.8)
07	May.	05:49	1.3	39.708(0.011)	141.873(0.019)	45.8(1.7)
07	May.	11:48	2.1	39.710(0.011)	141.867(0.018)	45.1(1.6)
14	May.	13:54	2.2	39.655(0.017)	142.099(0.027)	44.1(2.5)
14	May.	20:02	1.6	39.712(0.014)	142.095(0.020)	33.8(2.3)
19	May.	10:38	1.3	39.702(0.019)	142.157(0.014)	37.8(1.8)
21	May.	12:22	2.2	39.757(0.009)	142.037(0.018)	53.7(1.3)
22	May.	06:57	2.8	39.680(0.015)	142.050(0.027)	44.8(2.8)
05	Jun.	11:53	2.4	39.651(0.012)	142.104(0.018)	42.9(1.7)
11	Jun.	11:34	2.0	39.773(0.016)	142.142(0.023)	32.5(3.5)
13	Jun.	14:16	1.5	39.774(0.007)	141.869(0.014)	52.0(1.1)
10	Jul.	14:58	1.0	39.735(0.025)	142.155(0.019)	36.2(2.8)
10	Jul.	15:55	3.0	39.746(0.013)	141.788(0.024)	54.5(2.4)
11	Jul.	22:53	1.0	39.773(0.012)	142.128(0.010)	32.4(1.6)
18	Jul.	21:42	1.1	39.651(0.017)	142.052(0.024)	32.9(2.5)

standard error for each parameter. The locations of hypocentres are accurate within 5 km or less. The gross state of the seismic activity in the upper mantle during this period may be perceived in the epicentre map of Figure 1(a), and in the cross-sectional illustration of the hypocentres of Figure 1 (b). Solid circles in the figures give the locations of the earthquakes analysed here, cross symbols indicating the nearby stations of the network used in this study.

The basic data used in this study are the seismic signals detected by the electro-magnetic seismographs of 1 sec with a sensitivity of 3 V/kine at the stations of **MYK** (Miyako), **KGJ** (Kitakami), **HMK** (Himekami), and **HSK** (Hashikami). Figure 2 gives the examples of seismograms at these stations. As is shown in the figures, the seismograms, in particular at **MYK**, usually show impulsive onsets of both P and S waves. The determination of the source parameters from the spectra for small earthquakes is in general difficult because of the strong effect of structural localities on the seismic waves. The epicentral distances to the stations for the earthquakes concerned are not so large compared with their focal depths, and the emergence of the seismic ray at the stations is considered nearly vertical. Therefore, the recorded seismic waves are not so much contaminated by scattering, and thus we have obtained the spectra of remark-ably simple shape. This leads to a good estimation of the spectral parameters of these small earthquakes.

The seismic signals are telemetered to Kitakami Sub-Centre (**KGJ**), and recorded on an *FM* data recorder through a delay unit of 8 bit resolution with 135 sampling points per second. The frequency response of the telemetering and recording system is assured to be flat from *DC* to 30 Hz. The playback of the signals is made on a rectified

Fig. 1 (a) Seismic activity in the upper mantle around **MYK** during the period from April to July of 1976. Solid circles represent the earthquakes analysed in this study. Cross symbols indicate the locations of the nearby stations used in estimating the source parameters of the earthquakes.
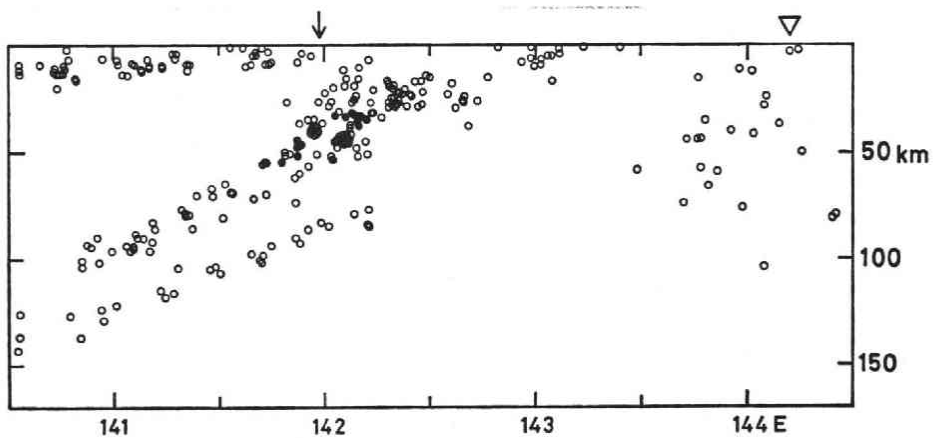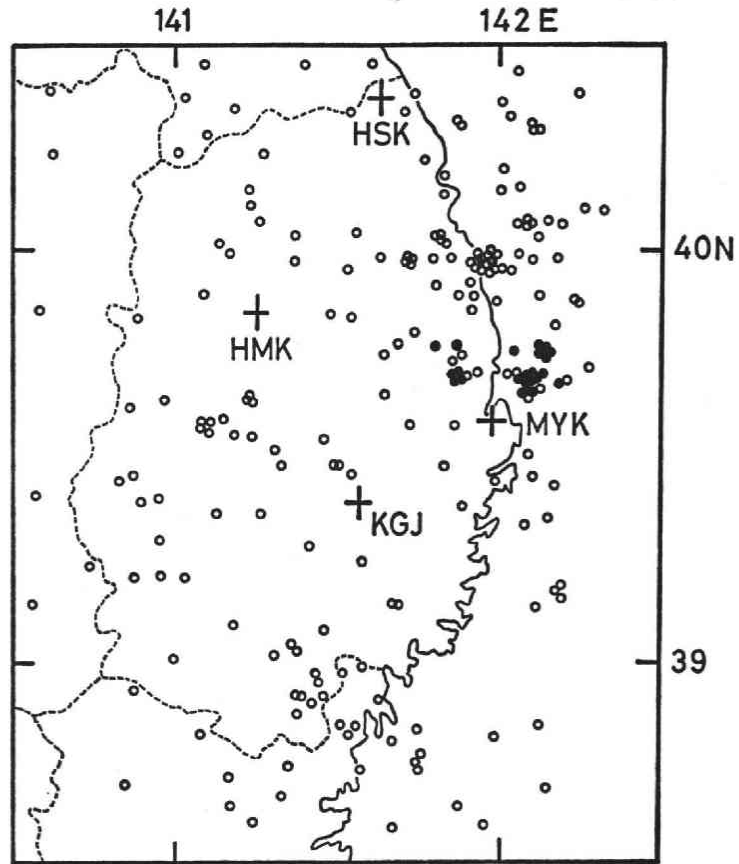
Fig. 1 (b) The projection of the hypocentres of the earthquakes on an E-W vertical cross-section for longitudes from 39°N to 40°N. Solid circles represent the earthquakes analysed in this study. The wedge symbol indicates the location of the trench, and the arrow the location of the station **MYK**. The epicentral distances of the earthquakes concerned with here to **MYK** are small compared with their focal depths.
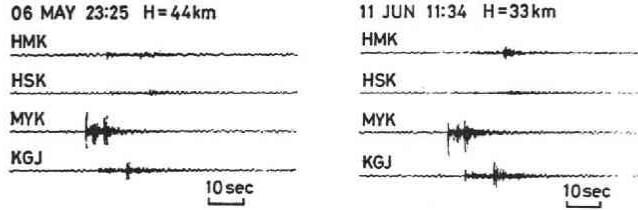
Fig. 2 The examples of the seismograms observed at the stations used in this study. The onsets of both P and S waves at **MYK** and at **KGJ** are implusive for these and many of the earthquakes.

pen-recorder with a 250 mm/sec chart speed, through 30 Hz low-pass filter which effectively eliminates the contamination by high-frequency tape noise. Two horizontal components of analogue signals are synthesized on the playback to yield an SH motion. The signal traces of P and SH waves are digitized with a scriptgraphic digitizer of 0.25 mm resolution at a sampling rate of about 250 Hz, at about 1 mm on actual trace. The digitized data are rearranged by the linear interpolation to get the values at the exact sampling rate of 250 Hz. Then the Goertzel algorithm is applied for the numerical integration to obtain an amplitude spectrum of displacement from the evaluation of

$$\varOmega(\omega) = \left| \frac{1}{\omega} \int_0^{t_0} \dot{g}(t) e^{-i\omega t} \, dt \right| , \tag{6}$$

where $\dot{g}(t)$ is a time series of ground velocity, t_0 the sample length.

A high sampling rate of 250 Hz is necessary for an accurate evaluation of spectral components at high frequencies. The sample lengths are fixed as 1 sec for both P and SH waves of all the events. The choice of this length is primarily due to the duration of signal without contaminative later phases. We have also examined the transfigura- tion of spectrum under a variety of sample lengths from 0.5 sec to 4.0 sec, to affirm that the spectrum suffers no significant change with sample lengths in this range, and consequently that a 1-sec sample length is sufficient and appropriate for an accurate determination of the low-frequency level $\varOmega_0$ and the corner frequency f_0 of the spectrum. The spectral lag window of the Hanning type is used to smooth the spectrum. The spectrum is corrected for the instrumental response of the seismograph, and for the frequency-independent free-surface response assuming a plane-wave incidence at the surface.

We have thus obtained the displacement spectrum which is distorted only by inelastic attenuation along propagation paths. The inelastic effect on the seismic waves is assumed to be of the form $\exp(-\pi ft/Q)$. A displacement source spectrum decays as $f^{-\gamma}$ beyond the corner frequency so that the ratio of observed sprctral component at $f_2(>f_1)$ to that at $f_1(>f_0)$ may be expressed as

$$\log \frac{\Omega_2}{\Omega_1} = -\gamma \log \frac{f_2}{f_1} - \pi \log e \frac{f_2 - f_1}{Q} t = -\gamma' \log \frac{f_2}{f_1} ,$$

$$\gamma' = \gamma + \pi \log e \frac{(f_2/f_1 - 1)}{\log(f_2/f_1)} \frac{f_1 t}{Q} > \gamma .$$

$$(7)$$

Then the observed displacement spectrum shows a steeper decrease at high frequencies than that due to the source effect itself. The observation of apparent decay γ' provides us with a way of evaluating the average Q values along various paths. Taking f_1 and f_2 as 15 Hz and 30 Hz, respectively, the equation (7) is then,

$$\gamma' = \gamma + \frac{68.3}{Q} t . \qquad (8)$$

The values of γ' at each station is plotted in Figure 3 as a function of travel time t. Although the plots in Figure 3 show some scatter, it is seen that there exists a tendency of increase in γ' with increasing tracel time t, except for at **MYK** where the values of γ' are larger for smaller travel times. The estimation of Q values from the observation of γ' requires an assumption on the value γ of the source spectral decay. According to Masuda et al., the source spectrum shows the f^{-2}-, or $f^{-1,5}$-decay beyond the corner frequency for P or S waves, respectively, at most azimuths. Assuming $\gamma = 2$ for P and $\gamma = 1.5$ for S waves, the average Q values are estimated at $600 \sim 800$ for P waves, and at $450 \sim 550$ for S waves along paths to **KGJ**, **HMK**, and **HSK**. These values agree well with those obtained by Suzuki (1974) and Umino and Hasegawa (1977) for the crust and upper mantle in the east side of the northeastern part of Honshu island, Japan. However, the attenuation effect along paths to **MYK** is more emphatic, the Q values being estimated at $300 \sim 400$ for both P and S waves. The estimate of smaller values for the paths to **MYK** may imply the structural locality around the station site
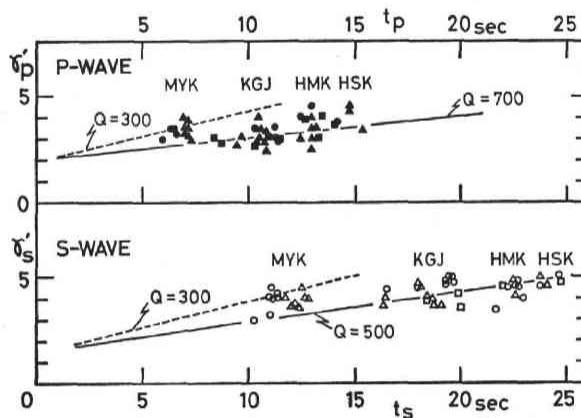

Fig. 3   The observed spectral decay γ' is plotted against travel time t for each station. Circles, triangles, and squares represent the data for the earthquakes with focal depths around 35 km, 45 km, and 55 km, respectively. The values observed at **MYK** are large for the smaller travel times.

06 MAY 23:25 H=44km

MYK P   Q=300

MYK S   Q=300
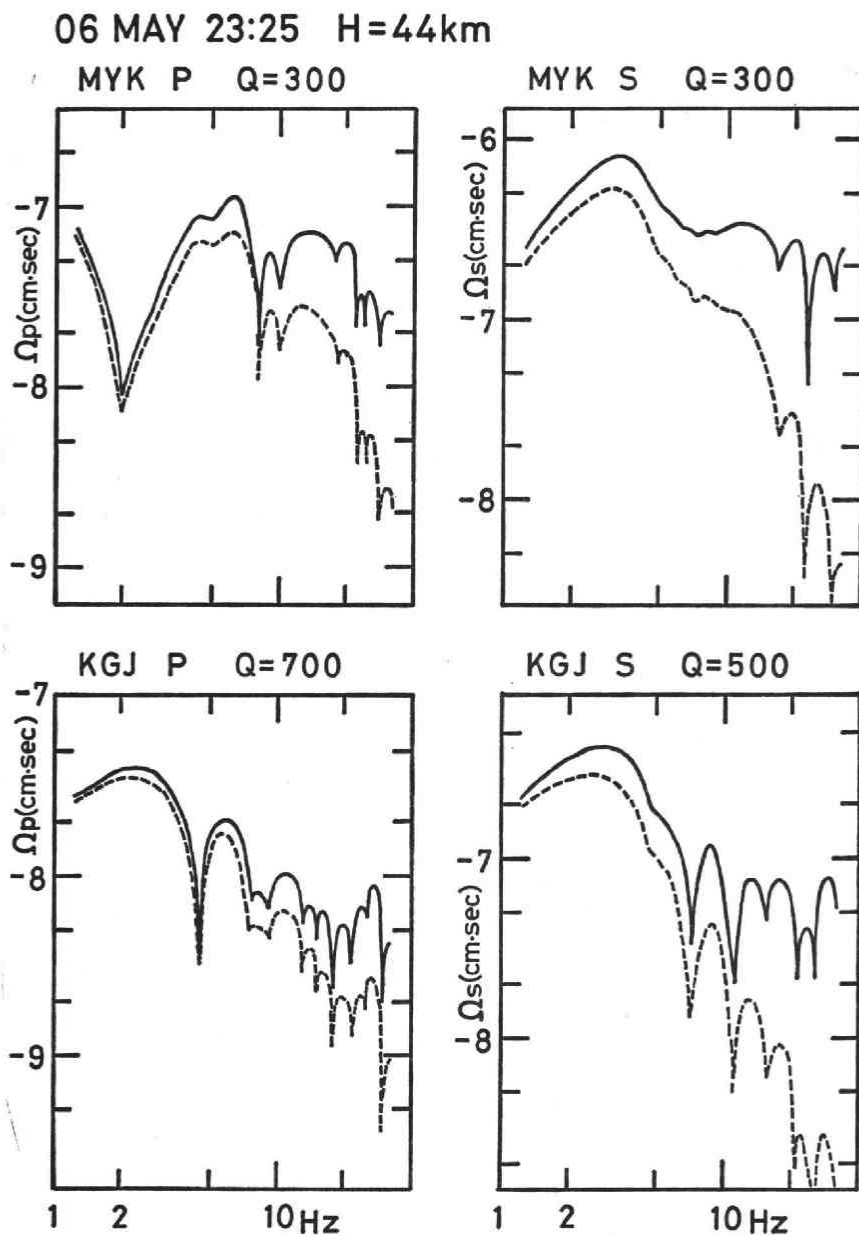
KGJ P   Q=700

KGJ S   Q=500

Fig. 4 (a) The observed spectra and the source spectra for the earthquakes shown in the left
column of Fig. 2. The source spectrum is obtained from the correction of the
observed spectrum for inelastic attenuation using the average Q value as shown. The
spectrum shows a pronounced decrease at high frequencies. The corner frequencies of
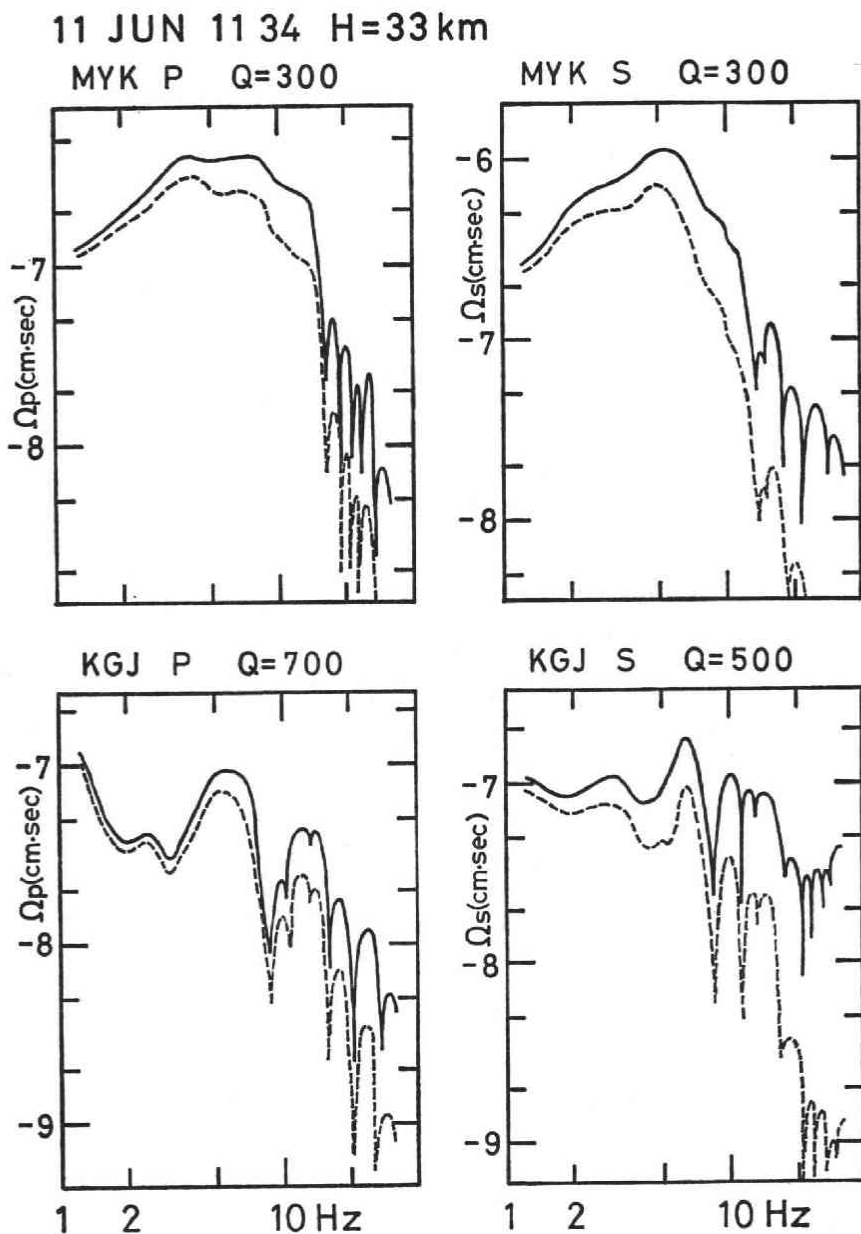P waves are larger than those of S waves.

11 JUN 11 34 H=33 km

Fig. 4(b)   The observed spectra and the source spectra for the earthquakes shown in the right column of Fig. 2.

and/or a strong contrast of the structure between the crust and upper mantle, because the seismic rays to **MYK** travel in the upper mantle only for a small distance, while the rays to **KGJ, HMK,** and **HSK** travel for comparatively large distances. Another interpretation of the difference in the estimates is attributing it to the wave contaminations. The seismic wave observed at **MYK** is less contaminated than those observed

at other stations, and the spectrum at **MYK** shows steeper decrease at high frequencies.

The observed spectra are corrected for inelastic attenuation assuming the Q values of 300 for both P and S waves along paths to **MYK**, and of 700 for P and 500 for S waves along paths to other stations. The example of the displacement spectra and source spectra are shown in Figure 4(a) and 4(b) for the earthquakes given in Figure 2. The examples show a pronounced decrease in amplitude with increasing frequency at high frequencies, the spectral corner clearly being identified. The spectra obtained in this study are easy to be interpreted in terms of low-frequency level Ω_0, corner frequency f_0, and high-frequency decay γ. The low-frequency level Ω_0 is determined within an error of a factor of 2 for each spectrum, and the corner frequency within 20 percent.

4. Source Parameters of the Earthquakes

We have determined the low-frequency level Ω_0 and the corner frequency f_0 of the spectra at the stations. From these basic parameters of Ω_0 and f_0, the source parameters of the earthquakes are estimated according to equations (1), (3), (4), and (5). The results are summarized in Table 2. Seismic moment M_0 is estimated at each station using the values $\rho=3.3$ g/cm, $\alpha=7.8$ km/sec, and $\beta=4.5$ km/sec. Since the fault plane solution of each earthquake is unknown, we have no reliable informations about radiation pattern coefficient $\mathscr{R}_{\theta\phi}$. The value of seismic moment reported in this paper is the average among the stations with $\mathscr{R}_{\theta\phi}=0.6$ for both P and SH waves of all the events. The fault radius R is also determined by averaging the values at the stations. The stress drop $\Delta\sigma$ is evaluated from the average values of M_0 and R.

Table 2.

| Date	h : m	m_{fp}	M_{0p} $\left(\begin{matrix}\text{dyne-cm}\\ \times 10^{20}\end{matrix}\right)$	f_{0p} (Hz)	R_p (km)	$\Delta\sigma_p$ (bars)	M_{0s} $\left(\begin{matrix}\text{dyne-cm}\\ \times 10^{20}\end{matrix}\right)$	f_{0s} (Hz)	R_s (km)	$\Delta\sigma_s$ (bars)
04 Apr.	19:48	2.1	0.40	10.0	.125	8.8	0.20	7.5	.094	10.4
07 Apr.	15:26	1.0	0.03	13.1	.095	1.5	0.04	8.0	.088	2.5
08 Apr.	19:54	1.5	–	–	–	–	0.05	10.0	.070	6.3
19 Apr.	08:00	1.9	0.12	12.0	.104	4.6	0.09	9.0	.078	8.2
20 Apr.	05:29	1.1	0.02	13.0	.096	1.0	0.03	12.0	.059	6.3
28 Apr.	16:27	3.0	8.00	6.0	.208	38.2	–	–	–	–
01 May.	17:09	1.3	0.10	14.0	.089	6.1	0.08	11.0	.064	13.1
06 May.	23:22	2.4	0.60	7.5	.166	5.6	0.20	5.0	.141	3.1
06 May.	23:25	2.2	0.10	7.5	.166	0.9	0.15	4.5	.156	1.7
07 May.	05:49	1.3	0.02	17.0	.073	2.2	0.03	15.0	.047	12.4
07 May.	11:48	2.1	0.06	15.0	.083	4.5	0.05	14.0	.050	17.2
14 May.	13:54	2.2	0.20	13.0	.096	9.7	0.10	8.0	.088	6.3
14 May.	20:02	1.6	0.20	13.0	.096	9.7	0.15	7.0	.101	6.3
19 May.	10:38	1.3	0.02	16.0	.078	1.8	0.03	9.5	.074	3.2
21 May.	12:22	2.2	0.20	11.0	.113	6.0	0.20	10.0	.070	25.1
22 May.	06:57	2.8	1.50	7.0	.178	11.4	–	–	–	–
05 Jun.	11:53	2.4	0.35	12.5	.100	15.1	0.15	11.0	.064	24.6
11 Jun.	11:34	2.0	0.40	11.0	.113	11.9	0.25	9.5	.074	26.5
13 Jun.	14:16	1.5	0.08	13.0	.096	3.9	0.06	11.0	.064	9.8
10 Jul.	14:58	1.0	0.05	13.5	.092	2.7	0.05	9.5	.074	5.3
10 Jul.	15:55	3.0	2.00	9.0	.139	32.0	–	–	–	–
11 Jul.	22:53	1.0	0.05	14.0	.089	3.1	0.02	10.0	.070	2.5
18 Jul.	21:42	1.1	0.04	15.0	.083	3.0	0.08	9.0	.078	7.3
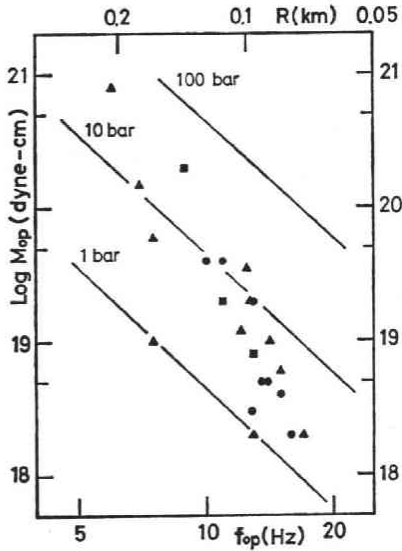
Fig. 5(a) M_0-f_0 diagram for the earthquakes and source parameters estimated from the P wave spectra. Circles, triangles, and squares represent the earthquakes with focal depths around 35 km, 45 km, and 55 km, respectively. f_0 corresponds to the fault radius scaled on the top of the figure. The straight lines of slope -3 indicate the constant stress drop.
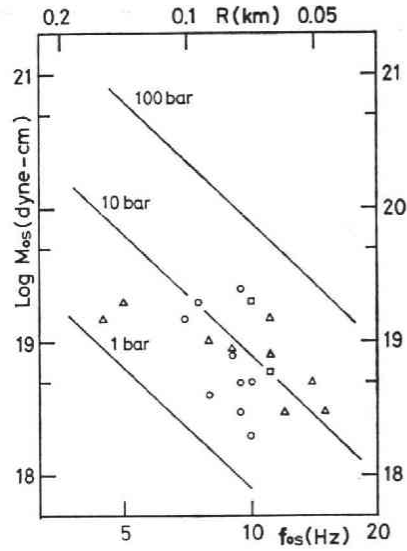
Fig. 5(b) M_0-f_0 diagram for the earthquakes and source parameters estimated from the S wave spectra. The meaning of each symbol is the same as in Fig. 5(a).

The M_0-f_0 diagrams obtained from P and S wave data are given in Figure 5(a) and 5(b), respectively. Circles represent the earthquakes with focal depths around 35 km, triangles around 45 km, and squares around 55 km. The symbols are used in the same meaning in all other figures in this paper. f_0 corresponds to the fault radius R scaled on the top of the figure. The straight lines with a slope of –3 stand for the constatnt stress drop with values indicated. The seismic moments of the earthquakes range from 10^{18} dyne-cm to 10^{21} dyne-cm, 10^3 dyne-cm being the upper limit of the dynamic range for available data in the present observation system. The absence of the S wave data for the earthquakes with seismic moments larger than 2.5×10^{19} dyne-cm is due to the saturation of signal. The fault radius R, ranging from 0.05 km to 0.2 km, increases with increasing seismic moment M_0 on the whole. The estimate from P waves gives somewhat larger values of fault radius than those from S waves. From equation (3) and (4), and with the values $a=7.8$ km/sec and $\beta=4.5$ km/sec, it is seen that the two estimates R_p and R_s coincide if $f_{0p}=1.6\,f_{0s}$. The systematical shift of R_p to larger values than R_s is due to the smaller ratios of f_{0p} to f_{0s} than 1.6. Figure 6 shows the ratio of P to S wave corner frequencies. It is found that the ratio falls within a range from 1.0 to 1.7, which agrees well with the theoretical prediction by Masuda et al. (1977a). The average value lies around $1.3 \sim 1.4$. The values of
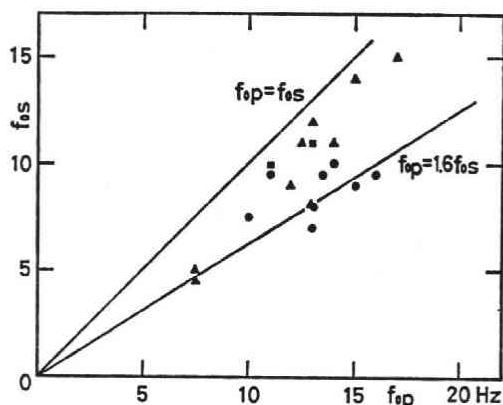
Fig. 6　The relation between the P wave corner frequencies, f_{op} and the S wave corner frequencies, f_{os}. The meaning of each symbol is the same as in the former figures. The ratio of P to S wave corner frequencies fall within a range from 1.0 to 1.7. The ratio is higher for the shallower earthquakes than for the deeper.
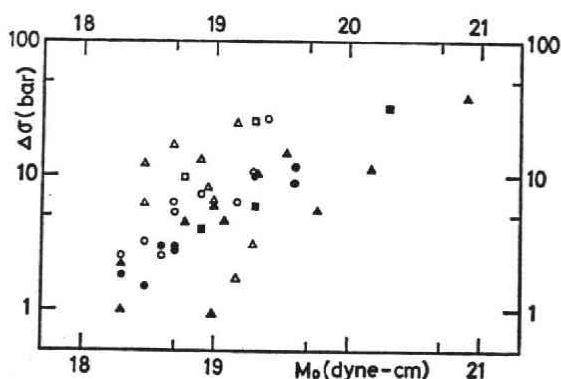

Fig. 7　The relation between stress drop and seismic moment of the earthquakes. The meaning of each symbol is the same as in Fig. 5. Solid symbols represent the P wave data, and open symbols the S wave data. Stress drops range from 1 bar to 40 bars. The P wave data insist on a linear log $\Delta\sigma$-log M_0 relation.

corner frequency for P waves higher than those for S waves have been expected from the study of pulse width in the time domain. The wave forms of P and S waves of the earthquakes are usually found very similar, but the pulse width of P waves is narrower than that of S waves.

In Figure 7, the stress drop $\Delta\sigma$ is plotted against the seismic moment M_0. Solid symbols represent the values estimated from P waves, and open symbols those from S waves. The stress drops range from 1 bar to 40 bars. The P wave data show a linear increase in log $\Delta\sigma$ with increasing log M_0, while the S wave data do not obviously show such a tendency. The P wave data give the slope of 0.6 for the earthquakes with seismic moments from 10^{18} dyne-cm to 5×10^{19} dyne-cm and stress drops from 1 bar to 10 bars. The slope appears to decrease for the earthquakes with seismic moments larger than 5×10^{19} dyne-cm and stress drops higher than 10 bars. The values

estimated from S waves are systematically larger than those estimated from P waves by a factor of 2 or 3. This discrepancy comes from the smaller estimates of fault radius R_s than R_p.

5. Discussions

We have obtained the seismic moment of an earthquake by averaging the estimates among the stations with $\mathscr{R}_{\theta\phi}=0.6$, since we have no reliable data to determine $\mathscr{R}_{\theta\phi}$. The uncertainty in the determination of $\mathscr{R}_{\theta\phi}$ is directly reflected on the uncertain estimat of seismic moment. One way of checking the reliability of estimated seismic moment is the comparison of the values obtained from P and S waves. Figure 8 illustrates the relation between the two estimates M_{0p} and M_{0s} for the earthquakes. The figure indicates an agreement between M_{0p} and M_{0s} within a factor of 2, which is compatible with an uncertainty in defining the flat level Ω_0 of the spectrum. Another independent way of the check is the study of the relation of seismic moment to earthquake magnitude. The magnitudes of the small earthquakes occurring in the northeastern Japan are determined from the total duration of signal by the Observation Centre for Earthquake Prediction, Tôhoku University, assuming the relation that

$$m_{fp} = a_0 + a_1 \log t_{fp} \tag{9}$$

where $a_1=3.0$ and $a_0=-2.9\sim-2.7$ depending upon station. The M_0-m_{fp} relation is shown in Figure 9, where solid symbols stand for the P wave data and open symbols for the S wave data. The result insists, in spite of the scatter of the data, on a linear relation of $\log M_0$ to m_{fp} expressed as

$$\log M_0 = 17.5 + 0.9 m_{fp} \tag{10}$$

for the earthquakes with seismic moments less than 5×10^{19} dyne-cm. For larger earthquakes, another relation seems to hold;

$$\log M_0 = 16.4 + 1.4 \log m_{fp} \tag{11}$$

though the data are not sufficient. The deviation of each value from the relation (10) or (11) is within a factor of 2 for most of the events. It may be concluded that the
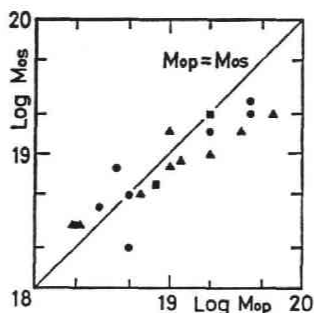

Fig. 8   The correlation between the two estimates, M_{0p} and M_{0s} of seismic moment are shown in order to check the reliability of these estimates. They agree with each other within a factor of 2.
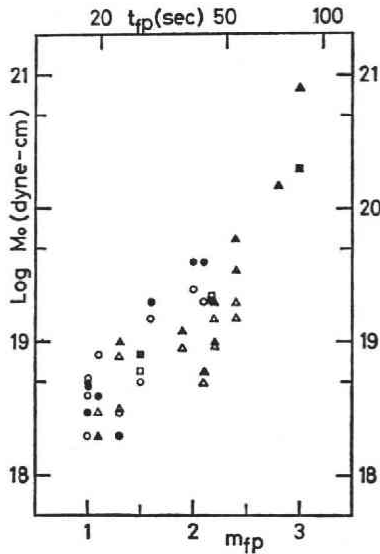
Fig. 9 Seismic moment estimated from the P wave spectra (solid) and from the S wave spectra
(open) is plotted against magnitude determined from the total duration of signal.   A
linear log moment-magnitude relation is indicated. The slope appears smaller for the
smaller earthquakes.

value obtained in this study gives a good estimate of seismic moment within a factor
of 2, and that the radiation directivity does not much affect the seismic moment
obtained for small earthquakes, as far as the average value among several stations is
concerned.

The corner frequencies are determined within the error of 20 percent. The
determination of corner frequencies for the earthquakes concerned are essentially
independent of the Q values used, since the spectra decrease pronouncedly beyond the
corner frequency. The ratio of P to S wave corner frequency is considered to be
accurate within an acceptable error of 30 percent. Our result that the P wave corner
frequencies are higher than the S wave corner frequencies is in accordance with those
by Molnar and Wyss (1972), Wyss and Molnar (1972), and Trifunac (1972). Bakun
et al. (1976), on the contrary, reported that the S wave corner frequencies are higher.
The difference in the ratio of P to S wave corner frequencies may be due to the
intrinsic differences in the source properties of fault geometry, source time function,
and rupture velocity (Savage, 1974; Dahlen, 1974; Burridge, 1975).

Since the seismic moment and the fault radius are determined within the error of a
factor of 2 and 20 percent, respectively, the stress drops are accurate within a factor of
5. Furthermore, the average deperture is rather less, about a factor of 3. The errors in
estimate, therefore, do not violate the results that the stress drops do not take a
constant value, but that there exists a tendency of increase in stress drop with increas-
ing seismic moment. It is of interest that the difference in stress drop is more than 1
order of magnitude for the small earthquakes in a narrow region, while almost the
constant stress drop is obtained for the large shocks with $M > 6$ (Kanamori and

Anderson, 1975; Geller, 1976). Our results suggest that the magnitude of small earthquakes scale with two factors of both R and $\Delta\sigma$. The fault length may be a dominant factor for the earthquakes in some region, but otherwise, the stress drop may more effectively give the measure of earthquake magnitude in another region. The dominance of one factor over the other may be due to an accidental condition in the source region.

Acknowledgements: We would like to thank Prof. Z. Suzuki for his kind advices throughout this study. We are greatly indebted to Prof. T. Hirasawa for his invaluable suggestions about the general understanding of the seismic source processes. The discussions with Drs. A. Hasegawa and N. Umino have been very helpful in the estimation of the Q values. Many thanks are due to all the staffs of Seismological Observatories of Tôhoku University for their providing us with comments on the data processing.

References

Bakun, W.H., C.G. Bufe, and R.M. Stewart, 1976: Body-wave spectra of central California earthquakes, Bull. Seism. Soc. Amer., **66**, 363–384.

Brune, J.N., 1970: Tectonic stress and the spectra of seismic shear waves from earhtquakes, J. Geophys. Res., **75**, 4997–5009.

Burridge, R., 1975: The effect of sonic rupture velocity on the ratio of S to P corner frequencies, Bull. Seism. Soc. Amer., **65**, 667–675.

Dahlen, F.A., 1974: On the ratio of P-wave to S-wave corner frequencies for shallow earthquake sources, Bull. Seism. Soc. Amer., **64**, 1159–1180.

Geller, R.J., 1976: Scaling relations for earthquake source parameters and magnitudes, Bull. Seism. Soc. Amer., **66**, 1501–1523.

Hanks, T.C. and M. Wyss, 1972: The use of bosy wave spectra in the determination of seismic-soruce parameters, Bull. Seism. Soc. Amer., **62**, 561–589.

Hasegawa, A., 1977; A study of deep seismic zone in the Northeastern Japan Arc, Dr. Thesis, Tohoku Univ.

Izutani, Y., 1974: Source parameters of some shallow earthquakes as derived from body waves, Master Thesis, Tohoku Univ.

Johnson, L.R. and T.V. McEvilly, 1974: Near-field observations and source parameters of central California earthquakes, Bull. Seism. Soc. Amer., **64**, 1855–1886.

Kanamori, H. and D.L. Anderson, 1975: Theoretical basis of some empirical relations in seismology, Bull. Seism. Soc. Amer., **65**, 1073–1095.

Keilis-Borok, V.I., 1959; On estimation of the displacement in an earthquake source and of source dimensions, Ann, Geofis. (Rome), **12**, 205–214.

Masuda, T., S. Horiuchi, and A. Takagi, 1977a: Far-field seismic radiation and its dependence upon the dynamic fracture process, Sci. Rep. Tôhoku Univ. Ser. 5, Geophys., **24**, 73–87.

Masuda, T., S. Horiuchi, and A. Takagi, 1977b: Dynamic features of expanding shear cracks in the presence of frictions, Sci. Rep. Tôhoku Univ. Ser. 5, Geophys., **24**, 55–72.

Molnar, P. and M. Wyss, 1972: Moments, source dimenstions and stress drops of shallow focus earthquakes in the Tonga-Kermadec Arc, Phys. Earth Planet Int., **6**, 263–278.

Sato, T. and T. Hirasawa, 1973: Body wave spectra from propagating shear cracks, J. Phys. Earth, **21**, 415–431.

Savage, J.C., 1974: Relation between P- and S-wave corner frequencies in the seismic spectrum, Bull. Seism. Soc. Amer., **64**, 1621–1627.

Suzuki, M., 1974; A study on deep and intermediate microearthquakes in the Tohoku district and seismic wave attenuation beneath the Northeastern Japan Island Arc, Dr. Thesis, Tôhoku Univ.

Takagi, A. and A. Hasegawa, 1976: Seismic Activity in the Northeastern Japan island arc system and study of earthquake prediction, in Proceedings of the National Symposium on Earthquake Prediction Researches, Dec. Tokyo, pp. 15–20.

Thatcher, W. and T.C. Hanks, 1973: Source parameters of southern California earthquakes, J. Geophys. Res., **78**, 8547–8576.

Trifunac, M.D., 1972: Stress estimates for the San Fernando, California earthquake of February 9, 1971: Main event and thirteen aftershocks, Bull. Seism. Soc. Amer., **62**, 721–750.

Trifunac, M.D., 1974: A three-dimensional dislocation model for the San Fernando, California earthquake of February 9, 1971, Bull. Seism. Soc. Amer., **64**, 149–172.

Umino, N. and A. Hasegawa, 1977; On inelastic attenuation of seismic body waves in Northeastern Japan, presented in the annual meeting of Seism. Soc., Japan, Tokyo.

Umino, N., A. Hasegawa, and A. Takagi; 1976; A detailed study on the deep seismic zone in Northeastern Japan, presented in the annual meeting of Seism. Soc., Japan, Tokyo.

Wyss. M. and P. Molnar, 1972: Source parameters of intermediate and deep focus earthquakes in the Tonga Arc, Phys. Earth Planet Int., **6**, 279–292.